Eurasian Chem.-Technol. J. 28 (2026) 67–82
The journal of the Institute of Combustion Problems https://ect-journal.kz

https://doi.org/10.18321/ectj1684

Corrosion Inhibition of Carbon Steel in 1M HCl by *Glaucium flavum* Alkaloids: Experimental Evaluation, Theoretical Insights, and Surface Characterization

Habiba Soltani[1]*, Karima Hanini[1,2], Merzoug Benahmed[2,3], Sameh Boudiba[1], Kawther Chabbi[1,4], Hocine Laouer[5], Louiza Boudiba[1]

[1]Laboratory of Applied Chemistry and Renewable Energies (LACRE), Echahid Cheikh Larbi Tebessi University, Constantine Road, 12002, Tebessa, Algeria
[2]Laboratory of Bioactive Molecules and Applications (LMBA), Faculty of Exact Sciences, Natural and Life Sciences, Echahid Cheikh Larbi Tebessi University, Constantine Road, 12002, Tebessa, Algeria
[3]Laboratory of Biomolecules and Plant Breeding (LBPB), Larbi Ben M'hidi University, 04000 Oum El Bouaghi, Algeria
[4]Faculty of Science and Applied Sciences, Larbi Ben M'hidi University, 04000 Oum El Bouaghi, Algeria
[5]Laboratory for the Valorization of Natural Biological Resources (LVNBR), Ferhatabbas University, Setif 1, Algeria

Article info

Received:
2 October 2025

Received in revised form:
6 December 2025

Accepted:
23 February 2026

Keywords:
Glaucium flavum
Corrosion inhibitor
Density functional theory
Electrochemical impedance
Surface morphology
Profilometry

Abstract

The corrosion inhibition of carbon steel (CS) in a 1 M HCl solution using the alkaloid extract from *Glaucium flavum* (AEGF) was investigated through a comprehensive and rigorous approach, including weight-loss measurements, potentiodynamic polarization, and electrochemical impedance spectroscopy (EIS). The results demonstrate that the inhibition efficiency of AEGF increases with concentration, reaching a maximum value of 81% at 200 ppm, but decreases at elevated temperatures. Potentiodynamic polarization studies reveal that AEGF acts as a mixed-type inhibitor, affecting both anodic and cathodic reactions. The adsorption behavior of the extract follows the Langmuir adsorption isotherm model. Thermodynamic parameters, including the apparent activation energy, enthalpy, and entropy of the dissolution process, were also evaluated, confirming that the inhibition mechanism is predominantly physisorption. The results obtained from different methodologies were consistent and mutually corroborative. In addition, surface analysis by scanning electron microscopy (SEM) coupled with energy-dispersive spectroscopy (EDS) showed that samples treated with the extract exhibited a smoother surface compared with untreated samples. This smoother surface morphology indicates reduced corrosion due to the decreased exposure of the metal surface to the corrosive medium, which was further confirmed by profilometry analysis. A theoretical study based on conceptual density functional theory (DFT) was also conducted to predict the reactive sites of the molecules. These predictions were based on the analysis of both local and global chemical reactivity indices.

1. Introduction

Steel, a versatile and essential material in modern society, is the backbone of construction, transportation, manufacturing, and numerous other applications [1]. However, the durability of this material is under constant threat from corrosion, which can pose serious risks ranging from aesthetic degradation to catastrophic structural failure [2]. To combat this, among the numerous techniques available, inhibitors are widely used. Corrosion inhibitors are substances used to protect materials by reducing the rate of corrosion when they are exposed to aggressive environments, such as acids, during pickling, descaling, and similar operations [3, 4].

The urgency of finding effective corrosion inhibitors is underscored by the critical role steel plays in our daily lives. This study aims to contribute to this urgent need by exploring the potential of *Glaucium flavum* extract as a corrosion inhibitor.

*Corresponding author.
E-mail address: habiba.habiba@univ-tebessa.dz

In recent decades, plant extracts have attracted considerable interest as eco-friendly corrosion inhibitors due to their abundant supply of natural chemical compounds [1–5]. These extracts, which can be extracted using simple methods at minimal cost and are naturally biodegradable [6], offer a promising avenue for sustainable corrosion prevention. The inhibiting action of plant extracts is frequently attributed to the adsorption of organic constituents onto the metal surface, which can obstruct active sites or even form a protective barrier [7, 8]. Alkaloids, a class of organic compounds that contain at least one nitrogen atom, have been shown to have potential as corrosion inhibitors due to their structure and properties [9–11].

This eco-friendly approach to corrosion prevention offers hope for a more sustainable future in materials science and engineering. One of the most extensively researched species in the genus Glaucium is the yellow horn poppy, *Glaucium flavum*, which belongs to the Papaveraceae family and is notable for its high alkaloid content [12–14]. The plant, which is native to Northern Africa, Western Asia, and Europe, exhibits a variety of therapeutic properties, including antioxidant, antitussive, bronchodilator, and hypoglycemic activities [15]. However, its potential as an anti-corrosion agent has not yet been fully explored. This study aims to fill this gap by evaluating the alkaloid extract of *Glaucium flavum* as a corrosion inhibitor for carbon steel in 1M HCl solution. The alkaloids were extracted from the plant using a process that ensures the purity and consistency of the extract. Gravimetric and electrochemical techniques were employed to assess inhibition performance, while SEM/EDS and profilometry were used to analyze surface morphology. Additionally, density functional theory (DFT) quantum chemical calculations were conducted to provide theoretical insights into the inhibition mechanism, potentially revealing a new, eco-friendly solution to the age-old problem of steel corrosion.

To better position this study within corrosion protection approaches, the advantages and limitations of using *Glaucium flavum* alkaloid extracts compared to conventional methods are briefly outlined. Compared to synthetic inhibitors, plant-based extracts are often cost-effective and readily available, making them attractive for sustainable corrosion control. Furthermore, the effective inhibition achieved at a relatively low concentration of 200 ppm highlights the extract's strong efficiency. However, natural inhibitors may present variability in composition depending on extraction methods and plant sources, which can affect reproducibility and inhibition efficiency. This study explores *Glaucium flavum* alkaloids as a promising green alternative while acknowledging these challenges.

2. Experimental

2.1. Protocol of extraction

The plant was harvested at the end of May 2022, according to GPS coordinates 36°20'03''N, 5°24'48''E, altitude 1107 m (Setif, Algeria), and identified by the esteemed Dr. LAOUER Hocine (Biology Department, Ferhat Abbas University, Setif 1, Algeria). One kilogram of dried and ground aerial parts was moistened with 500 mL of 28% ammonia diluted in half. The free bases were then solubilized in dichloromethane. The filtrate was evaporated under reduced pressure to obtain a concentrated extract in gel form. The next step was purification, which consists of using acid-base extraction to pass the alkaloids from the organic phase to the aqueous phase by acidification (adding diluted hydrochloric acid, 1M HCl), and vice versa from the aqueous phase to the organic phase via alkalinization (treating the obtained aqueous phase with NH_4OH until the pH reached around 9–10), allowing the removal of soluble impurities from both phases. The dichloromethane was then added to the basified aqueous solution, and the resulting organic phase was dried with Na_2SO_4, and then concentrated to dryness to obtain the *Glaucium flavum* alkaloid extract (AEGF) [9, 16].

2.2. Electrolytic solution

The electrolytic solution, a crucial component of our experiment, was meticulously prepared by diluting analytical-grade HCl with distilled water to obtain 1M HCl. To this, we added precise concentrations of AEGF to ensure the accuracy of our experimental conditions.

2.3. Material

All experiments were conducted using carbon steel (CS) specimens with the following chemical composition (wt%): C, 0.26%; Mn, 1.35%; P, 0.03%; S, 0.03%; and Fe as the balance.

2.4. Electrochemical measurements

The electrochemical tests were performed at room temperature (20 ± 1 °C) using an Origaflex 500 (OGF 500) potentiostat-galvanostat operated by an Origamaster 5. The setup included a platinum wire

serving as the counter electrode, a saturated calomel electrode (SCE) as the reference electrode, and API 5L-X60 carbon steel with an approximate surface area of 1 cm^2 as the working electrode.

Before each measurement, the working electrode was immersed for 30 min at open-circuit potential (OCP) to ensure OCP reached a steady state. The EIS experiments were conducted with a signal amplitude perturbation of 10 mV and a frequency range of 100 kHZ to 100 mHz, collecting 20 points per decade. The inhibition efficiency η_R (%) was calculated using Eq. 1 [17].

$$\eta_R(\%) = \frac{R_{ct} - R_{ct}^o}{R_{ct}} \cdot 100 \quad (1)$$

where R_{ct}° and R_{ct} are the charge transfer resistances for uninhibited and inhibited samples respectively.

Potentiodynamic polarization measurements were performed in the ± 250 mV potential range at a sweep rate of 1 mV/s. The inhibition efficiency η_P (%) was calculated using the equation below (Eq. 2) [17].

$$\eta_P(\%) = \frac{i_{corr}^o - i_{corr}}{i_{corr}^o} \cdot 100 \quad (2)$$

where i_{corr}° and i_{corr} are the corrosion current densities values in the absence and presence of the inhibitor, respectively.

2.5. Weight loss studies

The weight-loss measurement was used to assess the ability of each AEGF concentration to inhibit corrosion. The clean samples were weighed both before and after being suspended for 2 h at various temperatures in an aerated stagnant electrolytic solution. The weight change was meticulouslyrecorded and subsequently utilized to calculate the corrosion rate and inhibition efficiency η_w (%) using Eqs. 3 and 4, respectively [2].

$$CR = \frac{W}{At} \quad (3)$$

$$\eta_W(\%) = \frac{CR^o - CR}{CR^o} \cdot 100 \quad (4)$$

where *w* refers to the average weight loss, *t* represents the duration of immersion, Adenotes the total surface area of a single CS specimen, *CR*° and *CR* are the corrosion rates in the absence and presence of inhibitors, respectively.

2.6. Scanning electron microscopy with energy dispersive spectroscopy (SEM/EDS)

Following the immersion of the substrates in 1M HCl solution, both without and with the optimal concentration of AEGF for 2 h at 293 K, a comprehensive examination of the surface morphology of the CS specimens was conducted using SEM coupled with EDS (Thermo Scientific).

2.7. Theoretical analysis

Recent advancements in the development of exchange-correlation functions have enabled density functional theory (DFT) to accurately model complex interactions, such as the adsorption of inhibitor molecules on metal surfaces, particularly in the context of corrosion protection [18].

The adsorption property of inhibitor molecules is contingent on their capacity to donate or accept electrons. In this regard, dicentrine, bulbocapnine, and salutaridine, the major constituents reported in the whole plant extract of *Glaucium flavum* (Fig. 1) [19, 20], were selected as prime candidates for an in-depth theoretical investigation. Their molecular structures and electronic properties provided the foundation for computational modeling, offering valuable insights into their inhibition mechanisms at the metal-solution interface, with potential practical applications in the development of corrosion inhibitors.

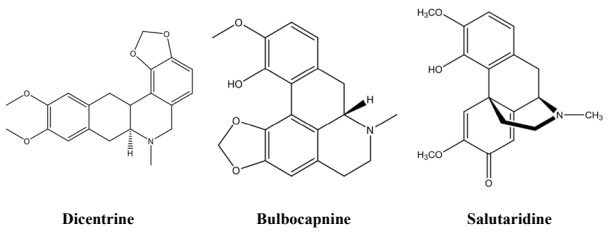

Fig. 1. Molecular structures of major alkaloid constituents from *Glaucium flavum*.

DFT was employed to provide information on electronic descriptors, such as the distribution of electron density in frontier molecular orbitals. It also allows the calculation of the energy of the highest occupied molecular orbital (E_{HOMO}), the lowest unoccupied molecular orbital (E_{LUMO}), their energy difference (ΔE), the ionization potential (I), the electron affinity (A), electronegativity (χ), overall softness (σ), hardness (η), and dipole moment, all in a relatively short time. DFT also allows the fraction of electrons transferred between molecules and metal (ΔN_{max}) to be obtained. The equations used to calculate these electronic parameters are as follows [21, 22].

$$\Delta E = E_{\mathrm{LUMO}} - E_{\mathrm{HOMO}} \quad (5)$$

$$\mathrm{I} = -E_{\mathrm{HOMO}} \quad (6)$$

$$A = -E_{\mathrm{LUMO}} \quad (7)$$

$$\chi = -\frac{1}{2}(E_{\mathrm{HOMO}} + E_{\mathrm{LUMO}}) \quad (8)$$

$$\eta = -\frac{1}{2}(E_{\mathrm{HOMO}} - E_{\mathrm{LUMO}}) \quad (9)$$

$$\sigma = \frac{1}{\eta} \quad (10)$$

$$\Delta N_{\max} = \frac{\chi}{2\eta} \quad (11)$$

These parameters help to understand the ability of corrosion inhibitors to donate and accept electrons on the metal surface [23].

The estimation of the electronic density distribution at the atomic level can be determined using Fukui indices (f_k), which are based on the fundamental principles of frontier orbital theory. These indices, known for their reliability, provide a robust representation of local chemical reactivity. They are used to identify potential reactive sites within a molecule, with a particular emphasis on those sites that exhibit vulnerability to nucleophilic, electrophilic, or radical attacks. The most common method for calculating these indices is based on Mulliken population analysis.

Theoretically, the Fukui function is defined as the first derivative of the electron density ρ(r) with respect to the number of electrons N, at a constant external potential v(r), according to the following equation:

$$f(r) = \left(\frac{\partial \rho(r)}{\partial N}\right)_{\mathrm{v(r)}} \quad (12)$$

In practical calculations, this function is generally approximated by finite differences in atomic charges between the neutral, anionic, and cationic states [24, 25], a method that is both reliable and feasible.

For a nucleophilicattack:

$$f^{+\mathrm{k}} = q_{\mathrm{k}}(N + 1) - q_{\mathrm{k}}(N) \quad (13)$$

For an electrophilicattack:

$$f^{-k} = q_{\mathrm{k}}(\mathrm{N}) - q_{\mathrm{k}}(\mathrm{N} - 1) \quad (14)$$

3. Results and discussion

3.1. Open circuit potential

Figure 2 illustrates the changes in open circuit potential (Eocp) of carbon steel in a 1 M HCl solution at 298 K, both in the absence and presence of different concentrations of AEGF. With the addition of AEGF, the OCP appears to increase over time and then gradually remain constant, shifting in a noble direction, indicating that AEGF controls mainly anodic metal dissolution reactions [26]. This gradual stabilization of OCP over time reassures us about the reliability of our results.

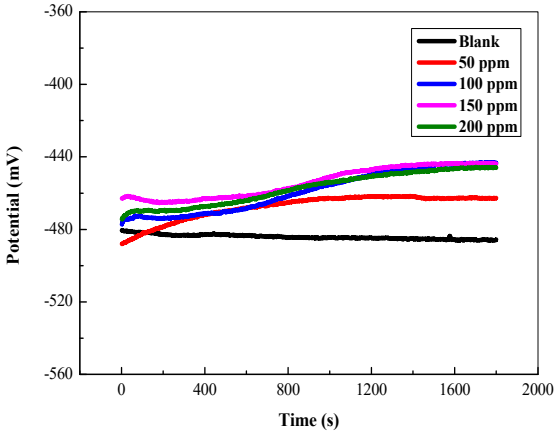

Fig. 2. Change in open circuit potential as a function of immersion time in 1 M HCl with and without different AEGF concentrations.

3.2. Potentiodynamic polarization measurements

Figure 3 illustrates the potentiodynamic polarization curves of CS in 1 M HCl solution both in the absence and presence of different concentrations of AEGF.

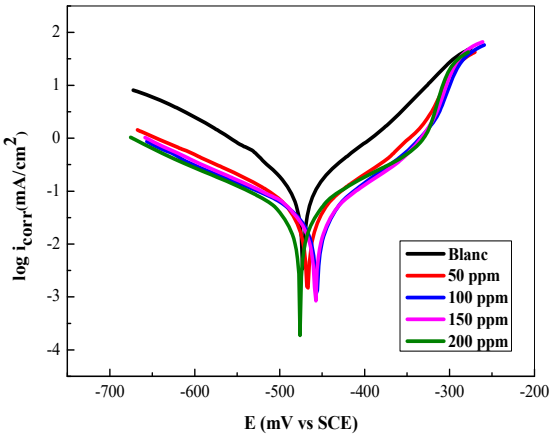

Fig. 3. CS's potentiodynamic polarization curves in 1 M HCl, both with and without different concentrations of AEGF.

Table 1. Corrosion polarization parameters for carbon steel in 1 M HCl solution without and with different concentrations of AEGF.

C (ppm)	$-E_{corr}$ (mV/SCE)	i_{corr} (mA/cm^2)	β_a (mV Dec^{-1})	$-\beta_c$ (mV Dec^{-1})	η_P (%)
0	472.5	0.1430	75.9	101.0	/
50	467.3	0.0423	59.4	126.8	70.42
100	456.3	0.0357	86.1	154.8	75.03
150	458.0	0.0337	97.7	136.4	76.03
200	475.9	0.0314	105.1	133.2	78.04

By analyzing Fig. 3, it has been found that introducing various concentrations of AEGF to 1 M HCl influences the cathodic and anodic parts of the curves, causing reduced current densities. This finding underscores the potential for inhibiting steel surface corrosion through inhibitor adsorption, which is responsible for the impact of extracts on both cathodic and anodic reactions in an acidic medium [2, 27].

According to the results presented in Table 1, the corrosion current density declines with increasing inhibitor concentration until it reaches a minimum of 0.0314 mA/cm^2 at 200 ppm, at which the inhibitory efficiency impressively reaches 78.04%. The increase indicates that inhibitor molecules from the extract form an adsorbed layer on the carbon steel surface, thereby inhibiting the corrosion process [28]. It is also worth noting that the displacement of the E_{corr} is less than 85 mV, demonstrating the inhibitor's mixed nature [29]. Additionally, the values for β_a and β_c do not follow a consistent pattern of increase or decrease, which reflects the mixed inhibition mode [30].

3.3. Electrochemical impedance spectroscopy (EIS)

Figure 4 displays Nyquist plots of a carbon steel electrode in 1 M HCl solution with and without different AEGF concentrations.

As shown in Fig. 4, the impedance spectra exhibit only one capacitive loop, indicating that steel corrosion is primarily controlled by a charge-transfer process [4]. Moreover, deviations of Nyquist plots from a perfect semicircle are typically attributed to frequency dispersion and surface inhomogeneities [31]. The addition of AEGF to the corrosive solution does not affect the appearance of the impedance plot, suggesting that the carbon steel experiences a similar corrosion process [32]. However, when varied AEGF concentrations are added to the aggressive solution, the Nyquist plot diameter increases, indicating enhanced corrosion resistance for the metal. This intriguing observation suggests that the presence of inhibitor molecules, possibly adsorbed on the metal surface, plays a significant role in this process [31, 32].

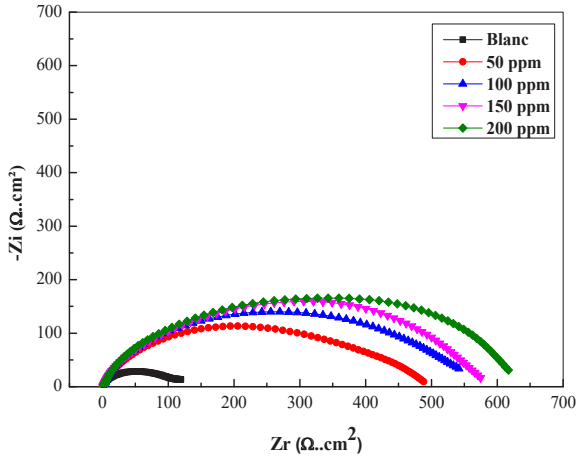

Fig. 4. Nyquist diagrams for CS in 1 M HCl solution with and without different AEGF concentrations.

The Nyquist plot was carefully analyzed by fitting it to an electrical equivalent circuit (EEC) model using EC LAB software. This circuit was selected for its superior fit to the Nyquist data at all inhibitor concentrations, an essential step in our study, as shown in Fig. 5. This model provides a comprehensive understanding of the electrochemical behavior of the system, enhancing our insights into the corrosion process.

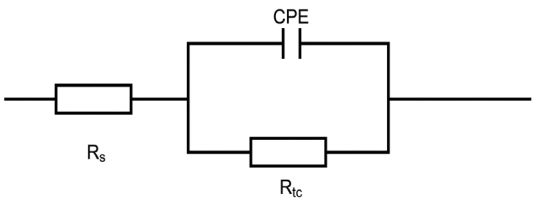

Fig. 5. Equivalent circuit used to fit Nyquist plots.

Table 2. Impedance parameters for carbon steel corrosion in 1 M HCl solution without and with varying concentrations of AEGF.

C (ppm)	R_{ct} (Ω.cm²)	10^{-5} Q ($S^n\Omega^{-1}$ cm^{-2})	n	C_{dc} (μFcm^{-2})	η_R (%)
0	119.2	77.8	0.572	132.30	/
50	484.3	25.9	0.0586	60.27	75.39
100	544.0	20.1	0.6080	48.60	78.09
150	579.9	15.7	0.6500	43.53	79.44
200	628.9	15.0	0.6500	42.32	81.05

The EEC consists of both the solution resistance and the charge transfer resistance. It's important to note that surface imperfections influence the double-layer capacitance value, which we simulate using a constant phase element (CPE) [27]. This CPE, a key element in our research, allows us to accurately model the double-layer capacitance. By applying the provided Eq. (15), the values of the double-layer capacitance (C_{dl}) are calculated [5].

$$C_{\mathrm{dl}} = R_{\mathrm{ct}}^{\frac{1-\mathrm{n}}{\mathrm{n}}} \times Q^{\frac{1}{\mathrm{n}}} \qquad (15)$$

where *n* is the deviation parameter of the CPE: $0 \le n \le 1$, and *Q* is the magnitude of CPE identified with the capacity.

Table 2 showcases the electrochemical parameters and inhibition efficiency η (%), which we determined using electrochemical impedance spectroscopy and the equivalent circuit. We specifically focused on different concentrations of AEGF, as they play a crucial role in our research.

Based on the data in Table 2, it was observed that the charge transfer resistance (R_{ct}) values increased with the rise in inhibitor concentration. This increase was significant, reaching a peak of 81.05% at 200 ppm, indicating that the inhibitor molecules provided substantial surface coverage through strong bonding to the metal surface [33]. Simultaneously, the double-layer capacitance (C_{dl}) values decreased, a result of the adsorption of inhibitor molecules onto the carbon steel surface, leading to the formation of a protective film that limits the number of active corrosion sites [9, 28].

3.4. Weight loss studies

Table 3 summarizes the values of inhibition efficiency η_w (%) and corrosion rate CR obtained from the weight loss method at various inhibitor concentrations and temperatures. As shown in Table 3, along with Figs. 6 and 7, increasing the inhibitor concentration leads to a significant reduction in the CR, a clear indication of the inhibitor's effectiveness η_w (%) in reducing corrosion. The highest corrosion inhibition efficiency was 85.39% obtained at 200 ppm.

As per the literature [34, 35], the significant improvement in corrosion inhibition at higher inhibitor concentrations is primarily due to the adsorption of inhibitor molecules onto the metal surface. This process effectively reduces the rate of metal dissolution, thereby lowering the corrosion rate. Conversely, the increase in corrosion rate with higher temperatures is a result of the accelerated metal dissolution process, making the metal more susceptible to corrosion.

Table 3. Corrosion parameters derived from weight loss measurements of carbon steel in 1 M HCl solution with varying concentrations of AEGF at different temperatures.

	293 K			303 K			313 K			323 K		
C_{ppm}	CR	θ	η_w (%)	CR	θ	η_w (%)	CR	θ	η_w (%)	CR	θ	η_w (%)
Blanc	0.1376	-	-	0.2049	-	-	0.2530	-	-	0.3793	-	-
50	0.0464	0.6628	66.28	0.0843	0.5886	58.86	0.1182	0.5328	53.28	0.1958	0.4838	48.38
100	0.0378	0.7252	72.52	0.0716	0.6505	65.05	0.1019	0.5972	59.72	0.1698	0.5523	55.23
150	0.0307	0.7769	77.69	0.0607	0.7037	70.37	0.0886	0.6498	64.98	0.1553	0.5907	59.07
200	0.0201	0.8539	85.39	0.0490	0.7608	76.08	0.0808	0.6806	68.06	0.1410	0.6282	62.82

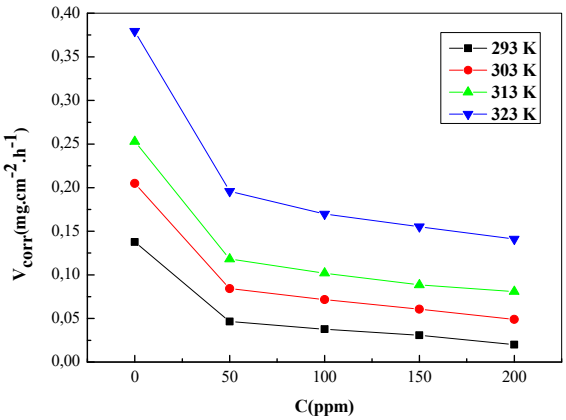

Fig. 6. Corrosion rate variation as a function of different AEGF concentrations in a 1 M HCl solution at different temperatures.

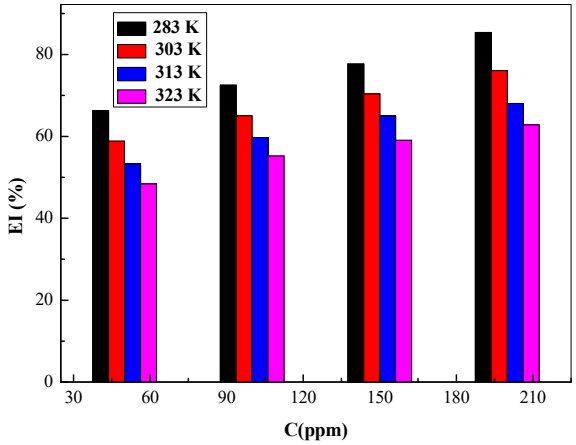

Fig. 7. Influence of temperature and concentration on the efficiency of AEGF inhibition in a 1 M HCl solution.

3.5. Adsorption isotherm

Langmuir, Temkin, and Freundlich isotherms were tested to determine the type of adsorption corresponding to the current study; the best graphical fit was found with Langmuir, according to the following equation [36]:

$$\frac{C}{\theta} = \frac{1}{K_{\text{ads}}} + C \qquad (16)$$

where θ is the surface coverage, C is the inhibitor concentration, and K_{ads} the equilibrium constant of the adsorption process.

The equilibrium constant of the adsorption process (K_{ads}) was determined from the intercept of the Langmuir isotherm plot shown in Fig. 8. Table 4 shows a decrease in K_{ads} values as temperature increases, suggesting that the inhibitors may be desorbing from the metal surface [2].

Table 4. Parameters of linear regression.

Temperature (K)	r^2	K_{ads} (l.mg^{-1})
293	0.9878	0.03666
303	0.9923	0.03292
313	0.9977	0.03263
323	0.9974	0.02882

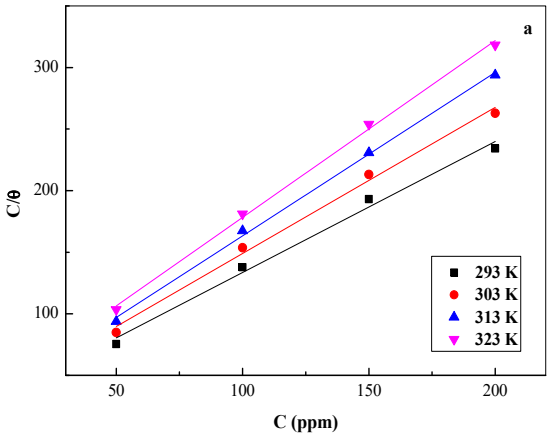

Fig. 8. Langmuir adsorption isotherm of AEGF on the CS in 1 M HCl solution at different temperatures.

3.6. Thermodynamic parameters

The standard Gibbs free energy of the adsorption process can be calculated based on the relationship given in the equation below [3]:

$$\Delta G°_{\text{ads}} = -RT \ln\left(C_{\text{H}_2\text{O}}.K_{\text{ads}}\right) \qquad (17)$$

where *R* is the gas constant, *T* is the absolute temperature (K) and C_{H_2O} is the concentration of water expressed in mg l^{-1} with an approximate value of 10^6 [17].

From Van't Hoff equation we can calculate the standard adsorption enthalpy ($\Delta H°_{ads}$) as follow [34]:

$$\frac{\mathrm{d}\ln K_{ads}}{\mathrm{d}T} = \frac{\Delta H°_{ads}}{RT^2} \qquad (18)$$

Equation (19) can be rewritten as [37]:

$$\ln K_{\text{ads}} = -\frac{\Delta H°_{\text{ads}}}{RT} + I \qquad (19)$$

where I is a constant of integration.

The value of ($\Delta H°_{ads}$) can be calculated from the linear plot of ln K_{ads} versus the inverse of temperature, where the slope represents $-\frac{\Delta H°_{ads}}{R}$ (Fig. 9).

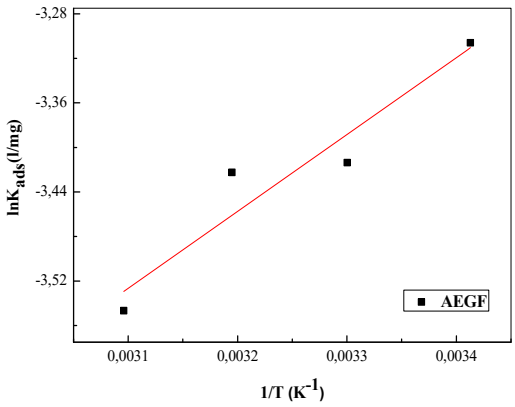

Fig. 9. Variation of ln K_{ads} as a function of the inverse of the temperature.

The standard adsorption entropy $\Delta S°_{ads}$ values are determined using the Gibbs-Helmholtz equation [4].

$$\Delta S°_{ads} = \frac{\Delta H°_{ads} - \Delta G°_{ads}}{T} \quad (20)$$

Table 5 displays the thermodynamic parameters. The data reveal that all values of the $\Delta G°_{ads}$ are negative, which suggests that the adsorption on the carbon steel surface occurs spontaneously [28]. Typically, the values of $\Delta G°_{ads}$ that are -20 kJ mol^{-1} or less negative point towards electrostatic interactions between charged molecules and charged metal surfaces [38]. In this study, the calculated values of $\Delta G°_{ads}$ ranged from -25.60 kJ mol^{-1} to -27.57 kJ mol^{-1}, clearly demonstrating that the extract undergoes physical adsorption on the metal surface across various temperatures [39]. This data is of significant importance in understanding the adsorption process.

Table 5. Standard thermodynamic parameters of AEGF adsorption in 1M HCl solution.

Temperature (K)	$\Delta G°_{ads}$ (kJ mol^{-1})	$\Delta H°_{ads}$ (kJ mol^{-1})	$\Delta S°_{ads}$ (J mol^{-1}K^{-1})
293	-25.60		67.78
303	-26.20	-5.738	67.53
313	-27.04		68.05
323	-27.57		67.59

The thermodynamic adsorption parameter values are not just numbers they provide profound insights into corrosion inhibition. An endothermic adsorption process ($\Delta H°_{ads} > 0$) is typically associated with chemisorption, whereas an exothermic adsorption process ($\Delta H°_{ads} < 0$) may involve either physisorption or chemisorption [39, 40]. In our investigation, the $\Delta H°_{ads}$ value is -5.738 kJ mol^{-1}. This outcome indicates the exothermic adsorption, confirming the earlier finding of the extract's physical adsorption on the steel surface. This revelation opens up new avenues for understanding and potentially controlling corrosion.

The positive adsorption entropy observed for AEGF is a fascinating aspect of the adsorption process. It can be explained by the quasi-substitution process in which inhibitor molecules replace water molecules adsorbed on the steel surface. However, it's not just substitution, but also an increase in the disorder caused by reactant formation at the metal/solution interface, which is responsible for inhibitor compounds adsorbing to metal surfaces [41, 42]. This disorder plays a significant role in the adsorption process, sparking curiosity and further research.

3.7. Activation parameters of the corrosion process

The activation energy is calculated using the Arrhenius Eq. (21) [43]

$$\ln CR = -\frac{E_a}{RT} + \ln D \quad (21)$$

where E_a is the apparent activation energy, and D is the Arrhenius pre-exponential factor.

Figure 10 shows a significant correlation between the temperature of the 1 M HCl solution and the logarithm of the corrosion rate (ln CR), both with and without the addition of extract. The slopes of the straight lines $-\frac{E_a}{R}$, determined for various inhibitor concentrations, are instrumental in calculating the apparent activation energies, a key finding in our study.

The activation energy values obtained in the present study, listed in Table 6,range from 36.67 kJ mol^{-1} and 50.05 kJ mol^{-1} in the presence of AEGF at various concentrations; these values are higher than the value obtained in the absence of the inhibitor, which is equal to 25.57 kJ mol^{-1}. The physical adsorption of the inhibitor on the steel surface explains the increase in activation energy, and the decrease in adsorption with increasing temperature is attributed to more inhibitor desorption at higher temperatures [44–46].

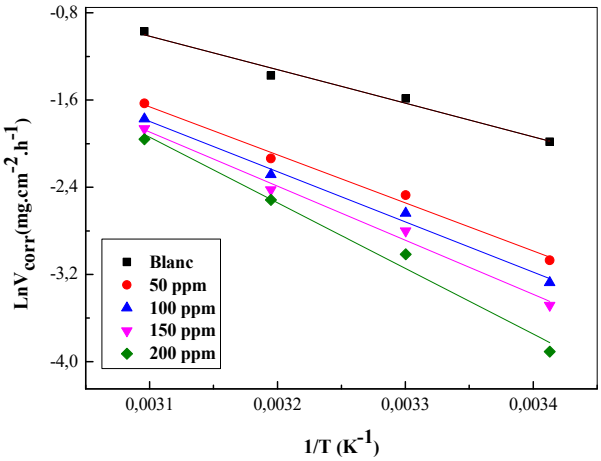

Fig. 10. Arrhenius plots of ln *CR* versus $\frac{1}{T}$ for CS corrosion in 1 M HCl of different concentrations of AEGF.

The activation enthalpy $\Delta H°_a$ and activation entropy ΔS_a of the corrosion process of CS in the acid medium can be calculated using an alternative Arrhenius formula (Eq. 22) [47]:

$$CR = \frac{RT}{N_a h} exp \frac{\Delta S°_a}{R} exp\left(-\frac{\Delta H°_a}{RT}\right) \quad (22)$$

where h is the Planck constant and N_a is the Avogadro number.

The variation of the $\ln\frac{CR}{T}$ as a function of the inverse of the temperature $\frac{1}{T}$ is a straight line (Fig. 11) with a slope of $-\frac{\Delta H^{\circ}_a}{R}$ and ordinate at the origin equals $\ln\frac{R}{N_a h}+\frac{\Delta S^{\circ}_a}{R}$.

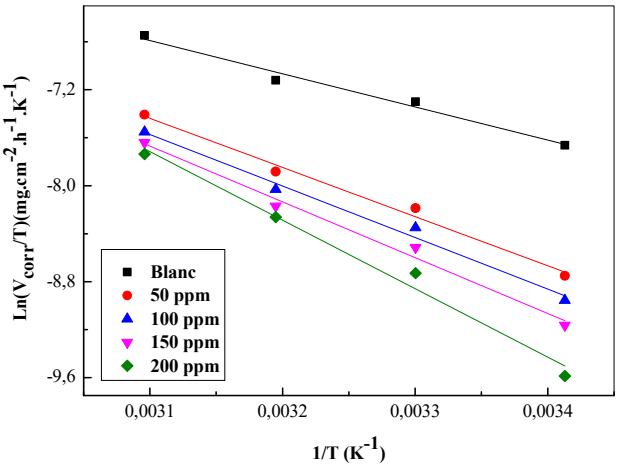

Fig. 11. Arrhenius plots of $\ln\frac{CR}{T}$ versus $\frac{1}{T}$ for CS corrosion in 1 M HCl of different concentrations of AEGF.

Table 6 presents the activation enthalpies and entropies. The positive enthalpy values, indicating the endothermic nature of the carbon steel dissolution process, carry significant implications for our understanding of corrosion processes [48]. Conversely, the activation entropy $\Delta S°_a$ for AEGF suggests that the rate-determining step involves an association rather than dissociation, implying a decrease in disorder [2].

Table 6. Activation parameters for CS in 1M HCl for different concentrations of AEGF.

C (ppm)	E_a (kJ mol^{-1})	ΔH_a (kJ mol^{-1})	$10^{-1}\ \Delta S_a$ (J mol^{-1} K^{-1})
0	25.57	23.02	-18.26
50	36.67	34.11	-15.36
100	38.28	35.72	-14.97
150	41.27	38.72	-14.12
200	50.05	47.50	-11.44

3.8. Scanning electron microscopy with energy dispersive spectroscopy (SEM/EDS)

SEM and EDS analyses were conducted to investigate the surface morphology of the carbon steel specimens and to determine the elemental composition of both corroded and inhibited metal surfaces. The morphologies, spectra, and chemical compositions obtained before and after 2 h of immersion in HCl solutions, with and without the inhibitor, are presented in Fig. 12 and Table 7.

Table 7. Chemical composition of CS immersed in 1 M HCl solution without and with the addition of 200 ppm AEGF.

		Fe	C	O	Cl
1 M HCl	wt%	94.37	2.20	3.37	0.06
	Atom %	81.05	8.77	10.10	0.08
AEGF	wt%	98.28	1.64	0.00	0.07
	Atom %	92.69	7.19	0.00	0.11

The SEM images of the specimens, showcased in Fig. 12, vividly depict the impact of the inhibitor on the rate of corrosion. In Fig. 12a, the surface of the CSis marred and rough, with pits caused by corrosion in the acidic medium. However, Fig. 12b provides a clear visual evidence of the inhibitor's role in reducing the rate of corrosion and surface damage. The formation of a protective inhibitor film on the CS surface is a key factor in this reduction [49].

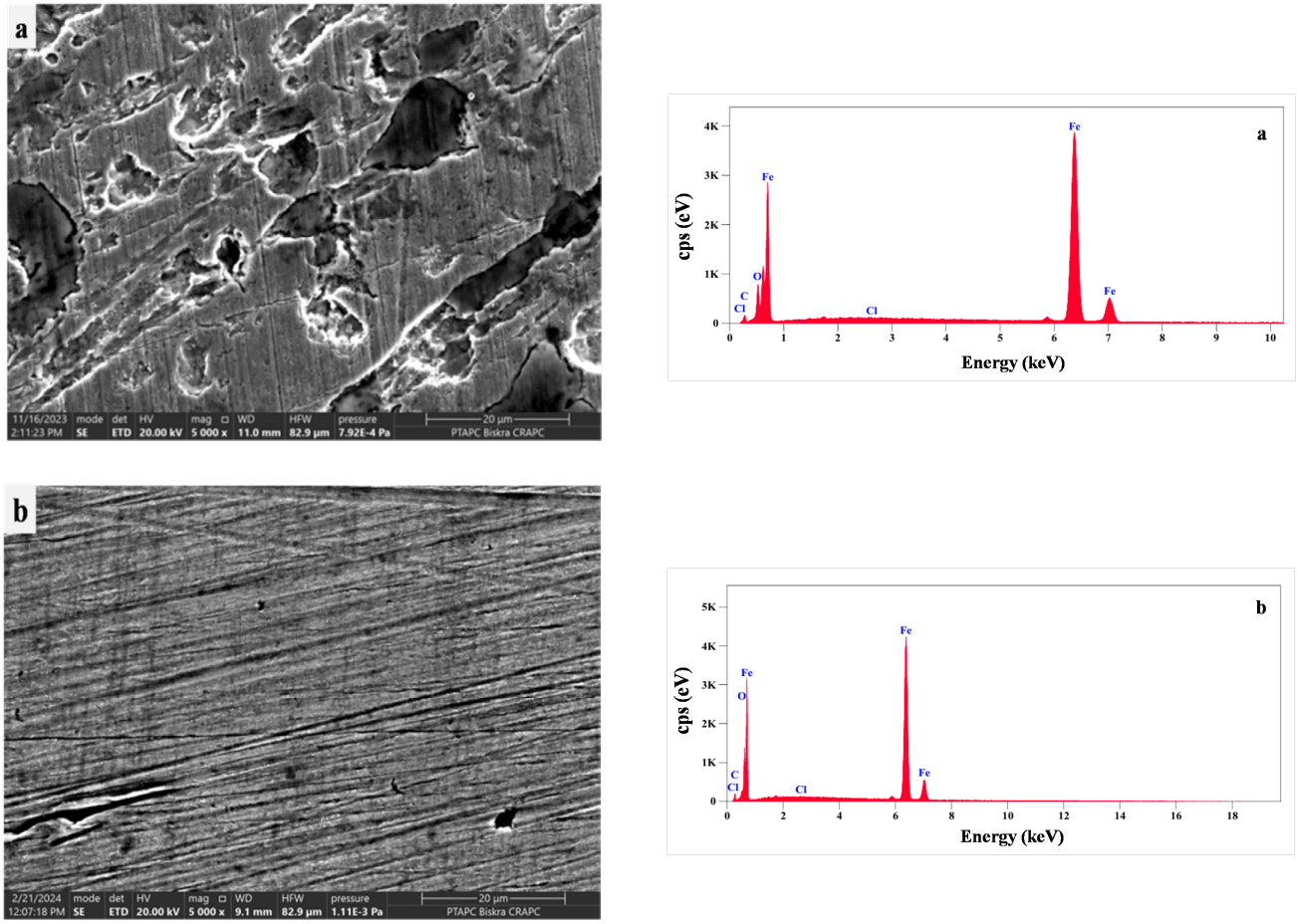

Fig. 12. SEM/EDS images of CS immersed in: a) 1 M HCl solution; and in 1 M HCl containing; b) 200 ppm AEGF.

In Fig. 12, the EDS spectra are presented, and in Table 7, the atomic percentage of various elements found on the surface of CS, inhibited and uninhibited, is provided. As shown in Fig. 12, the spectrum of the inhibited sample indicates that the Fe peaks are considerably more intense compared to the uninhibited CS sample. This increase in Fe content is a result of the inhibitor's role in reducing the dissolution of Fe, which in turn prevents the formation of iron oxides and hydroxides on the metal surface. The absence of the oxygen peak upon addition of the inhibitor further confirms this [49, 50].

3.9. Profilometer

To evaluate the inhibitory effect of AEGF on the steel surface, particularly in terms of surface roughness, a profilometer (AltiSurf 520) was used. Figure 13 and Table 8 present the 3D and 2D surface morphologies, together with the roughness parameters of carbon steel before and after immersion in 1 M HCl, both in the absence and presence of 200 ppm AEGF, for an immersion period of 2 h.

Before immersion, the steel surface appears relatively smooth, with only a few irregularities. After immersion in 1 M HCl, significant corrosion occurs, leading to the formation of pits and cavities that markedly increase the surface roughness. This increase is attributed to the corrosive action of hydrochloric acid, as evidenced by the significantly higher Sa value, indicating that the surface becomes considerably rougher. In contrast, when AEGF is added to the 1 M HCl solution, the Sa value decreases compared to the sample immersed in the acid alone. The reduction in surface roughness suggests that AEGF effectively inhibits the corrosion process. This behavior may be attributed to the formation of a protective layer on the steel surface, which limits the direct interaction between the acid solution and the metal surface.

Table 8. Surface roughness parameter.

	ISO 25178		
	Without immersion	1 M HCl	AEGF
Sa (µm)	2.34	5.24	4.64

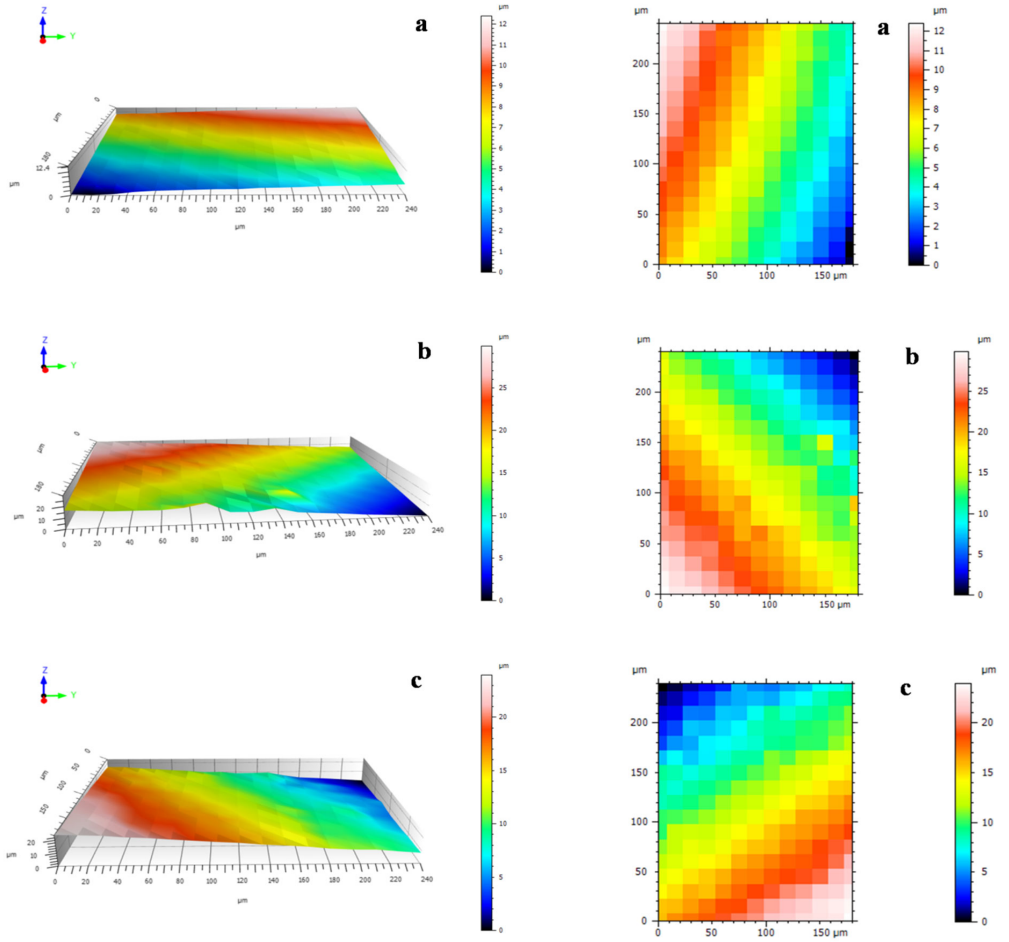

Fig. 13. 3D and 2D morphology of carbon steel surfaces: a) without immersion; b) immersion in a 1M HCl solution; c) in a 1M HCl solution containing 200 ppm of AEGF.

3.10. Theoretical analysis

A DFT study was conducted to investigate the electronic structure and chemical reactivity of the three main components (Salutaridine, Dicentrine, Bulbocapnine) previously isolated as principal constituents in earlier phytochemical investigations of different *Glaucium flavum* populations [19, 20]. The geometrically optimized structures, as well as the HOMO and LUMO, are presented in Table 9. It can be seen that for all three molecules, the distribution of the HOMO and LUMO electron densities is similar, with the HOMO orbitals delocalized over the aromatic parts, highlighting a high electron density on these structures. This indicates a significant ability to donate electrons, making these regions particularly susceptible to attack by electrophilic species, such as positively charged metal sites. While the LUMO orbitals are located on the oxygen and nitrogen functions, giving these molecules good reactivity potential of metal surfaces. These molecules are also evaluated for their potential as corrosion inhibitors, using quantum parameters related to their electronic reactivity, polarity, and ability to interact with a metal surface. The DFT calculations performed for the three molecules studied are summarized in Table 10. Based on these detailed results, the Salutaridine molecule has the lowest gap (3.82 eV), indicating a strong capacity to participate in electron-exchange reactions. Its highest dipole moment (7.58 D) suggests strong polarity, making it more likely to form bonds with polar metal surfaces such as steel. Furthermore, its moderate softness and high charge-transfer capacity (ΔN = 0.915) make it an excellent inhibitor candidate, capable of effectively adsorbing onto a metal surface and transferring electrons to it. This process is conducive to the formation of a protective layer against corrosion, a promising application of these compounds [52]. Although stable, dicentrine shows low reactivity. Bulbocapnine occupies an intermediate position.

Fukui's analysis, a key tool for understanding molecular reactivity, identified the most reactive sites responsible for the adsorption of the three molecules on the steel's active sites. For the molecule Salutaridine (Fig. 14), it has been found to have several notable electrophilic centers in its aromatic carbon skeleton on carbon atoms C6 (0.323), C14 (0.269), and C15 (0.267), which coincide with the location of the LUMO and indicate an ability to accept electrons from the metal. Nucleophilic reactivity is dominated by oxygenated heteroatoms and nitrogen with high f-values O20 (0.343), O19 (0.326), O26 (0.316), O31 (0.389), and N33 (0.310), which constitute preferential sites of interaction with the metal surface. In the case of Bulbocapnine (Fig. 15), carbon C24, which is highly electrophilic (dominant f^+ = 0.2913), constitutes the main acceptor center associated with the LUMO. At the same time, the HOMO density is distributed over several peripheral carbons (C28, C13, C6, and C5), which are identified as nucleophilic sites. This configuration suggests a localized adsorption site that can promote selective interactions with the metal. Finally, for Dicentrine (Fig. 16), Fukui indices indicate a carbon-based nucleophilic island (C16–C20) consistent with HOMO density, while the methoxy oxygens (O27, O29, O26), which are highly electrophilic (high f^+), coincide with the LUMO density areas.

Table 9. Optimized structures, and representation of molecular orbital HOMO/LUMO obtainedfromthe theoretical analysisusingDFT / B3LYP/6-311G(D,P).

Molecules	Structures	HOMO	LUMO
Salutaridine	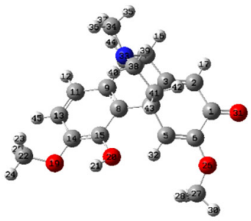	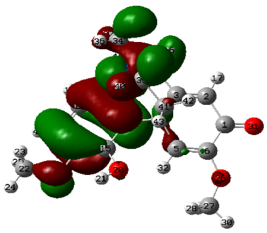	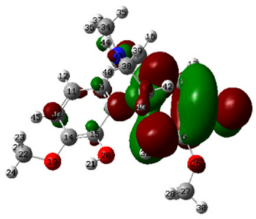
Bulbocapnine	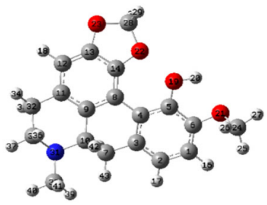	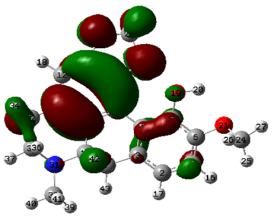	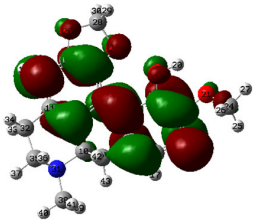
Dicentrine		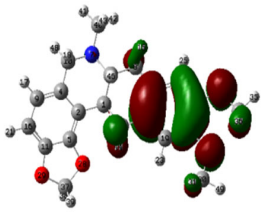	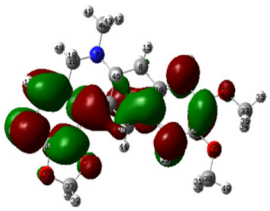

Table 10. Calculated quantum chemical parameters of Salutaridine, Bulbocapnine, and Dicentrine, obtained from theoretical analysis using DFT / B3LYP/6-311G(D,P).

Atomes	HOMO (eV)	LUMO (eV)	ΔE (eV)	I (eV)	A (eV)	μ (D)	X	η	S	ΔN
Salutaridine	-5.40309	-1.58368	3.81941	5.40309	1.58368	7.583368	3.493385	1.909705	0.52364109	0.91463996
Bulbocapnine	-5.35411	-0.90477	4.44934	5.35411	0.90477	2.553471	3.12944	2.22467	0.44950487	0.70334926
Dicentrine	-5.31656	-0.19755	5.11901	5.31656	0.19755	2.624187	2.757055	2.559505	0.39070055	0.53859145

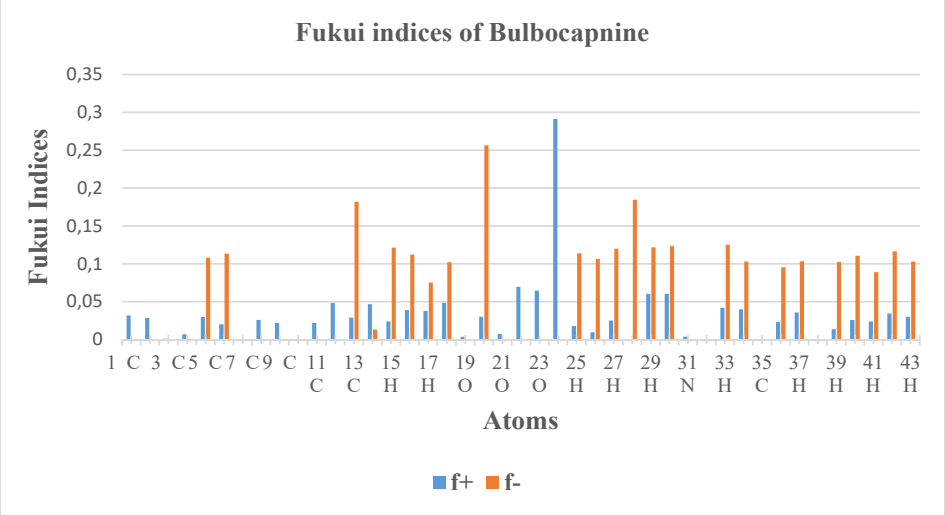

Fig. 15. Graphical representation of the predicted Fukui indices of Bulbocapnine.

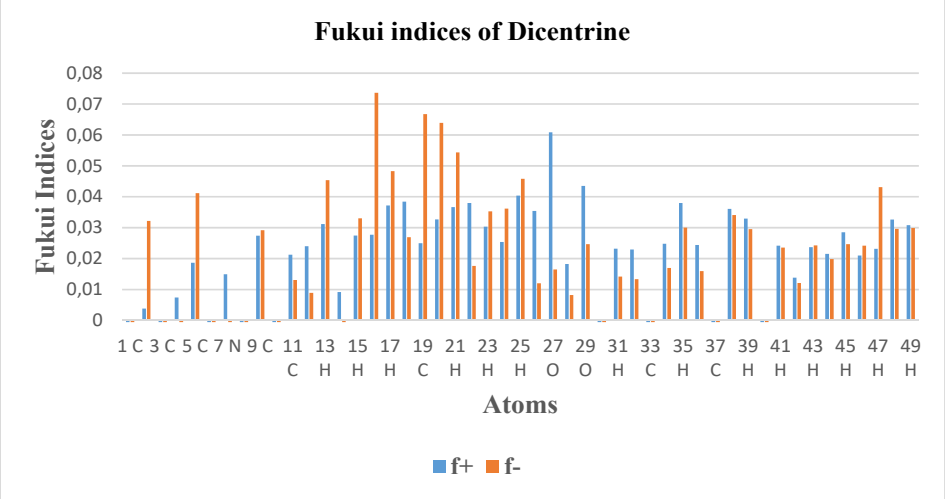

Fig. 16. Graphical representation of the predicted Fukui indices of Dicentrine.

4. Conclusion

The investigation into the corrosion inhibition of carbon steel (CS) in a 1 M hydrochloric acid (HCl) solution using alkaloid extracts from *Glaucium flavum* has yielded significant findings.

– Alkaloid extracts from *Glaucium flavum* demonstrated effective corrosion inhibition of carbon steel in 1 M HCl, reaching a maximum efficiency of 81% at 200 ppm, although the efficiency decreases with rising temperature.

– The adsorption of the extract follows the Langmuir isotherm and is characterized as physisorption, while the extract acts as a mixed-type inhibitor affecting both anodic and cathodic reactions.

– Surface analyses (SEM, EDS, and profilometry) confirmed the formation of a protective film on the steel surface, improving morphological characteristics compared to untreated samples.

– Quantum chemical studies (DFT) of key alkaloids, Salutaridine, Bulbocapnine, and Dicentrine, revealed complementary reactive sites and highlighted the importance of molecular electronic properties and metal interaction in determining inhibition efficiency.

In summary, the research has found that alkaloid extracts from *Glaucium flavum* can effectively inhibit the corrosion of carbon steel in hydrochloric acid solutions, with the potential for practical applications in corrosion control.

Acknowledgments

The authors gratefully thank Echahid Cheikh Larbi Tebessi University for supplying the necessary resources to conduct this research.

References

[1]. S. Boudiba, K. Hanini, I. Selatnia, et al., Experimental, theoretical and mathematical studies of Echium italicum L. extract as a corrosion inhibitor for carbon steel in acidic medium, *Mater. Res. Express* 6 (2019) 086546. DOI: 10.1088/2053-1591/ab194f

[2]. K. Hanini, M. Benahmed, S. Boudiba, et al., Influence of different polyphenol extracts of Taxus baccata on the corrosion process and their effect as additives in electrodeposition, *Sustain. Chem. Pharm.* 14 (2019) 100189. DOI: 10.1016/j.scp.2019.100189

[3]. H. Mahfoud, N. Rouag, S. Boudiba, et al., Mathematical and Electrochemical Investigation of Lamium flexuosum Extract as Effective Corrosion Inhibitor for CS in Acidic Solution Using Multidimensional Minimization Program System, *Arab. J. Sci. Eng*. 47 (2022) 6605–6616. DOI: 10.1007/s13369-021-06546-y

[4]. M. Benahmed, N. Djeddi, S. Akkal, et al., Saccocalyx satureioides as corrosion inhibitor for carbon steel in acid solution, *Int. J. Ind. Chem*. 7 (2016). 109–120. DOI: 10.1007/s40090-016-0082-z

[5]. A. Kalla, M. Benahmed, N. Djeddi, et al. Corrosion inhibition of carbon steel in 1 M H2SO4 solution by Thapsia villosa extracts, *Int. J. Ind. Chem*. 7 (2016) 419–429. DOI: 10.1007/s40090-016-0094-8

[6]. H. Soltani, K. Hanini, M. Benahmed, et al., Experimental and Surface Evaluation of Zinc Electroplating Efficiency and Corrosion Inhibition Effects of Centaurea napifolia Extracts, *Eurasian Chem.-Technol. J.* 27 (2025) 45–70. DOI: 10.18321/ectj1655

[7]. A. Ishak, F.V. Adams, J.O. Madu, et al., Corrosion inhibition of mild steel in 1M hydrochloric acid using Haematostaphis barteri leaves extract, *Procedia Manufacturing* 35 (2019) 1279–1285. DOI: 10.1016/j.promfg.2019.06.088

[8]. A. Thomas, M. Prajila, K.M. Shainy, et al., A green approach to corrosion inhibition of mild steel in hydrochloric acid using fruit rind extract of Garcinia indica (Binda), *J. Mol. Liq.* 312 (2020) 113369. DOI: 10.1016/j.molliq.2020.113369

[9]. K. Hanini, M. Benahmed, S. Boudiba, et al., Experimental and Theoretical Studies of Taxus Baccata Alkaloid Extract as Eco-Friendly Anticorrosion for Carbon Steel in Acidic Solution, *Prot. Met. Phys. Chem. Surf*. 57 (2021) 222–233. DOI: 10.1134/S2070205120060118

[10]. N.El. Hamdani, R. Fdil, M. Tourabi et al., Alkaloids extract of Retama monosperma (L.) Boiss. seeds used as novel eco-friendly inhibitor for carbon steel corrosion in 1 M HCl solution: Electrochemical and surface studies, *Appl. Surf. Sci*. 357 (2015) 1294–1305. DOI: 10.1016/j.apsusc.2015.09.159

[11]. A. Lecante, F. Robert, P.A. Blandinières, et al., Anti-corrosive properties of S. tinctoria and G. ouregou alkaloid extracts on low carbon steel, *Curr. Appl. Phys.* 11 (2011) 714–724. DOI: 10.1016/j.cap.2010.11.038

[12]. V. Petitto, M. Serafini, F.R. Gallo, et al., Alkaloids from Glaucium flavum from Sardinia, *Nat. Prod. Res*. 24 (2010) 1033–1035. DOI: 10.1080/14786410902904418

[13]. L. Bournine, S. Bensalem, P. Peixoto, et al., Revealing the anti-tumoral effect of Algerian Glaucium flavum roots against human cancer cells, *Phytomedicine* 20 (2013) 1211–1218. DOI: 10.1016/j.phymed.2013.06.007

[14]. A.M. Arafa, M.E.S. Mohamed, S.I. Eldahmy, The aerial parts of yellow horn poppy (Glaucium flavum Cr.) growing in Egypt: isoquinoline alkaloids and biological activities, *J. Pharm. Sci. Res.* 8 (2016) 323–332.

[15]. T. Akaberi, K. Shourgashti, S.A. Emami, et al., Phytochemistry and pharmacology of alkaloids from Glaucium spp, *Phytochemistry* 191 (2021) 112923. DOI: 10.1016/j.phytochem.2021.112923

[16]. A. Djilani, B. Legseir, R. Soulimani, et al., New extraction technique for alkaloids, *J. Braz. Chem. Soc*. 17 (2026) 518–520. DOI: 10.1590/S0103-50532006000300013

[17]. X. Li, S. Deng, H. Fu, Inhibition of the corrosion of steel in HCl, H2SO4 solutions by bamboo leaf extract, *Corros. Sci.* 62 (2012) 163–175. DOI: 10.1016/j.corsci.2012.05.008

[18]. F. Iorhuna, A.M. Ayuba, T.A. Nyijime et al., A DFT and Molecular Dynamic (MD) Simulation on the Adsorption of Vidarabine as a Potential Inhibitor on the Al Metal surface, *Adv. J. Chem. A* 6 (2023) 380–390. DOI: 10.48309/ajca.2023.409740.1390

[19]. I. Lalezari, A. Shafiee, M. Mahjour, Major alkaloids of Glaucium flavum Grantz, population Ghom, *J. Pharm. Sci.* 65 (1976) 923–924. DOI: 10.1002/jps.2600650633

[20]. A. Shafiee, I. Lalezari, S. Lajevardi, et al., Alkaloids of Glaucium flavum grantz, populations isfahan and kazerun, *J. Pharm. Sci.* 66 (1977) 873–874. DOI: 10.1002/jps.2600660636

[21]. S. Lavie, Y. Goshen, E. Kraisler, Ionization potentials and fundamental gaps in atomic systems from the Ensemble-DFT approach, *J. Chem. Phys*. 158 (2023) 154111. DOI: 10.1063/5.0142670

[22]. I.M.A. Omar, A.M. Al-Fakih, Effect of red clover

(Trifolium pratense L.) aqueous extract as an additive on nickel electrodeposition: Experimental and theoretical study, *Arab. J. Chem*. 2024, 105680. DOI: 10.1016/j.arabjc.2024.105680

[23]. I. Selatnia, A. Sid, M. Benahmed, et al., Synthesis and characterization of a bis-pyrazoline derivative as corrosion inhibitor for A283 carbon steel in 1M HCl: electrochemical, surface, DFT and MD simulation studies, *Prot. Met. Phys. Chem. Surf*. 54 (2018) 1182–1193. DOI: 10.1134/S2070205118060229

[24]. F. De Proft, J.M.L. Martin, P. Geerlings, Calculation of molecular electrostatic potentials and Fukui functions using density functional methods, *Chem. Phys. Lett*. 256 (196) 400–408. DOI: 10.1016/0009-2614(96)00469-1

[25]. K. Hanini, C. Kawther, S. Boudiba, et al., Effect of Beta vulgaris L. Extracts as an Additive on the Electrodeposition of Zinc on Mild Steel in Chloride Solution: Coating Characterization and Corrosion Behavior in Seawater, *Int. J. Electrochem. Sci.* 20 (2025) 101104. DOI: 10.1016/j.ijoes.2025.101104

[26]. M. Benahmed, I. Selatnia, N. Djeddi, et al., Adsorption and corrosion inhibition properties of butanolic extract of Elaeoselinum thapsioides and its synergistic effect with Reutera lutea (Desf.) Maires (Apiaceae) on A283 carbon steel in hydrochloric acid solution, *Chem. Afr.* 3 (2020) 251–261. DOI: 10.1007/s42250-019-00093-8

[27]. X. Li, S. Deng, H. Fu, Adsorption and inhibition effect of vanillin on cold rolled steel in 3.0 M H3PO4, *Prog. Org. Coat.* 67 (2010) 420–426. DOI: 10.1016/j.porgcoat.2009.12.006

[28]. E. Elqars, M. Guennoun, N. Sqalli Houssini, et al., The adsorption performance of chicken excrement extract as corrosion inhibition of carbon steel in a 1 M HCl medium, *J. Bio Tribo Corros.* 7 (2021) 1–12. DOI: 10.1007/s40735-021-00520-9

[29]. S. Saravanamoorthy, S. Velmathi, Physiochemical interactions of chiral Schiff bases on high carbon steel surface: Corrosion inhibition in acidic media, *Prog. Org. Coat.* 76 (2013) 1527–1535. DOI: 10.1016/j.porgcoat.2013.06.003

[30]. K.V. Kumar, M.S.N. Pillai, G.R. Thusnavis, Seed extract of Psidium guajava as ecofriendly corrosion inhibitor for carbon steel in hydrochloric acid medium, *J. Mater. Sci. Technol.* 27 (2011) 1143–1149. DOI: 10.1016/S1005-0302(12)60010-3

[31]. A. Döner, R. Solmaz, M. Özcan, et al., Experimental and theoretical studies of thiazoles as corrosion inhibitors for mild steel in sulphuric acid solution, *Corros. Sci.* 53 (2011) 2902–2913. DOI: 10.1016/j.corsci.2011.05.027

[32]. R. Solmaz, Investigation of adsorption and corrosion inhibition of mild steel in hydrochloric acid solution by 5-(4-Dimethylaminobenzylidene) rhodanine, *Corros. Sci.* 79 (2014) 169–176. DOI: 10.1016/j.corsci.2013.11.001

[33]. K. Muthukumarasamy, S. Pitchai, K. Devarayan, et al., Adsorption and corrosion inhibition performance of Tunbergia fragrans extract on mild steel in acid medium, *Mater. Today: Proc.* 33 (2020) 4054–4058. DOI: 10.1016/j.matpr.2020.06.533

[34]. N. Djeddi, M. Benahmed, S. Akkal, et al., Study on methylene dichloride and butanolic extracts of Reutera lutea (Desf.) Maire (Apiaceae) as effective corrosion inhibitions for carbon steel in HCl solution, *Res. Chem. Intermed.* 41 (2015) 4595–4616. DOI: 10.1007/s11164-014-1555-3

[35]. O.A. Akinbulumo, O.J. Odejobi, E.L. Odekanle, Thermodynamics and adsorption study of the corrosion inhibition of mild steel by Euphorbia heterophylla L. extract in 1.5 M HCl, *Results in Materials* 5 (2020) 100074. DOI: 10.1016/j.rinma.2020.100074

[36]. A. Kosari, M.H. Moayed, A. Davoodi, et al., Electrochemical and quantum chemical assessment of two organic compounds from pyridine derivatives as corrosion inhibitors for mild steel in HCl solution under stagnant condition and hydrodynamic flow, *Corros. Sci.* 78 (2014) 138–150. DOI: 10.1016/j.corsci.2013.09.009

[37]. P. Muthukrishnan, B. Jeyaprabha, P. Prakash, Adsorption and corrosion inhibiting behavior of Lannea coromandelica leaf extract on mild steel corrosion, *Arab. J. Chem*. 10 (2013) S2343–S2354. DOI: 10.1016/j.arabjc.2013.08.011

[38]. C.P. Kumar, K.N. Mohana, Corrosion inhibition efficiency and adsorption characteristics of some Schiff bases at mild steel/hydrochloric acid interface, *Taiwan Inst. Chem. Engrs*. 45 (2014) 1031–1042. DOI: 10.1016/j.jtice.2013.08.017

[39]. S.A. Umoren, U.M. Eduok, M.M. Solomon, et al., Corrosion inhibition by leaves and stem extracts of Sida acuta for mild steel in 1 M H2SO4 solutions investigated by chemical and spectroscopic techniques, *Arab. J. Chem*. 9 (2016) S209–S224. DOI: 10.1016/j.arabjc.2011.03.008

[40]. K. Tebbji, N. Faska, A. Tounsi, et al., The effect of some lactones as inhibitors for the corrosion of mild steel in 1 M hydrochloric acid, *Mater. Chem. Phys.* 106 (2007) 260–267. DOI: 10.1016/j.matchemphys.2007.05.046

[41]. X. Li, S. Deng, H. Fu, et al., Adsorption and inhibition effect of 6-benzylaminopurine on cold rolled steel in 1.0 M HCl, *Electrochim. Acta* 54 (2009) 4089–4098. DOI: 10.1016/j.electacta.2009.02.084

[42]. X. Li, S. Deng, H. Fu, et al., Synergistic inhibition effect of rare earth cerium (IV) ion and anionic surfactant on the corrosion of cold rolled steel in H2SO4 solution, *Corros. Sci*. 50 (2008) 2635–2645. DOI: 10.1016/j.corsci.2008.06.026

[43]. L. Bammou, M. Belkhaouda, R. Salghi, et al., Corrosion inhibition of steel in sulfuric acidic solution by the Chenopodium Ambrosioides Extracts, *J. Assn. Arab. Univ. Basic. Appl. Sci*. 16 (2014) 83–90. DOI: 10.1016/j.jaubas.2013.11.001

[44]. M.N. El-Haddad, Hydroxyethylcellulose used as an eco-friendly inhibitor for 1018 c-steel corrosion in 3.5% NaCl solution, *Carbohydr. Polym*. 112 (2014) 595–602. DOI: 10.1016/j.carbpol.2014.06.032

[45]. Y. El Ouadi, A. Bouyanzer, L. Majidi, et al. (2015) Evaluation of Pelargonium extract and oil as eco-friendly corrosion inhibitor for steel in acidic chloride solutions and pharmacological properties, *Res. Chem. Intermed*. 41 (2015) 7125–7149. DOI: 10.1007/s11164-014-1802-7

[46]. S. Martinez, I. Stern, Thermodynamic characterization of metal dissolution and inhibitor adsorption processes in the low carbon steel/mimosa tannin/sulfuric acid system, *Appl. Surf. Sci.* 199 (2002) 83–89. DOI: 10.1016/S0169-4332(02)00546-9

[47]. I.E. Uwah, P.C. Okafor, V.E. Ebiekpe, Inhibitive action of ethanol extracts from Nauclea latifolia on the corrosion of mild steel in H2SO4 solutions and their adsorption characteristics, *Arab. J. Chem*. 6 (2013) 285–293. DOI: 10.1016/j.arabjc.2010.10.008

[48]. M. Behpou, S.M. Ghoreishi, M. Khayatkashani, et al., Green approach to corrosion inhibition of mild steel in two acidic solutions by the extract of Punica granatum peel and main constituents, *Mater. Chem. Phys*. 131 (2012) 621–633. DOI: 10.1016/j.matchemphys.2011.10.027

[49]. A. Bouoidina, E. Ech-Chihbi, F. El-Hajjaji, et al., Anisole derivatives as sustainable-green inhibitors for mild steel corrosion in 1 M HCl: DFT and molecular dynamic simulations approach, *J. Mol. Liq*. 324 (2021) 115088. DOI: 10.1016/j.molliq.2020.115088

[50]. E.B. Caldona, M. Zhang, G. Liang, et al., Corrosion inhibition of mild steel in acidic medium by simple azole-based aromatic compounds, *J. Electroanal. Chem*. 880 (2021) 114858. DOI: 10.1016/j.jelechem.2020.114858

[51]. M.A.M. El-Haddad, A. Bahgat Radwan, M.H. Sliem, et al., Highly efficient eco-friendly corrosion inhibitor for mild steel in 5 M HCl at elevated temperatures: experimental & molecular dynamics study, *Sci. Rep.* 9 (2019) 3695. DOI: 10.1038/s41598-019-40149-w

[52]. A. Bouoidina, F. El-Hajjaji, K. Emran, et al., Towards understanding the anticorrosive mechanism of novel surfactant based on Mentha pulegium oil as eco-friendly bio-source of mild steel in acid medium: a combined DFT and molecular dynamics investigation, *Chem. Res. Chin. Univ.* 35 (2019) 85–100. DOI: 10.1007/s40242-019-8205-7